FORSCHUNG - AUSBILDUNG - WEITERBILDUNG

Bericht Nr. 36

OPTIMIZATION OF A SPRING FOR DENTAL ATTACHMENTS

Peter Hack, Claus-Peter Fritzen

UNIVERSITÄT KAISERSLAUTERN
Fachbereich Mathematik
Fachbereich Maschinenwesen
Erwin-Schrödinger-Straße
D - 6750 Kaiserslautern

Oktober 1989

OPTIMIZATION OF A SPRING FOR DENTAL ATTACHMENTS

Peter Hackh
Department of Mathematics
Claus-Peter Fritzen
Department of Applied Mechanics
University of Kaiserslautern
6750 Kaiserslautern, FRG

Abstract. Special technological applications like the construction of a dental attachment require structural parts which have very small overall dimensions. Very often these parts are subjected to high loadings. The failure of a small spring was the starting point for an investigation with the aim to design a suitable new spring shape.

1. INTRODUCTION

Structural failure occurs in almost any field of engineering application. Although failures of structural parts of artificial dentures are not perilous, they can be very troublesome for the patient.
One special problem in dental technology is to find a suitable attachment between the removable and the fixed part of the dental prosthesis. Some general demands for such an attachment are

- wide range of applicability, which is achieved especially by means of a space-saving design,
- no impairment of dental hygiene,
- no esthetical impairment,
- simple processing in dental laboratories,
- possible combination with other alloys used in dental technology,
- no maintenance, simple exchange,
- low cost.

For medical reasons a "rigid" connection which does not allow (even small) rotations of the prosthesis has to be preferred to a hinge connection.
An attachment satisfying these requirements is the recently developed "FR-Chip" by OBERSAT [1,2]. Beside other parts this chip consists of a small rectangular box, which contains a small spring with overall size of 5 mm × 3 mm × 0.4 mm bended from a spring wire (see fig. 1 and 2). This spring snaps into a groove and locks the fixed and the removable parts of the denture. The space saving incorporation of the chip is shown in fig. 3. Later the chip is plugged into (and fixed within) the dental prosthesis and is not visible.

Fig. 1: Chip-box and original spring of the FR-chip

Fig. 2: Schematic illustration of the spring position in the chip-box

---

Fig. 3: Application of the FR-chip in a dental prosthesis model

---

Due to the small overall dimensions as well as to the (relative) large spring deflection of 0.3 mm, the spring is exposed to very high loadings. The high stress level caused a fracture of the spring in many cases. For reasons of manufacturing tolerances in the dental laboratory, the spring deflection cannot be reduced furthermore.
The task was to find a well suited spring shape with the following feature:

- the spring has the same overall size as before so that the chip-box has not to be changed,
- the mechanical stresses are below an admissible value for a spring deflection of 0.3 mm,
- the elastiac spring force lies within a range of 1.2 and 2 N for that deflection,
- the spring can be produced by means of standard manufacturing methods.

Unfortunately, the demands for lower stresses and higher elastic forces are not compatible. The force needed to remove the dental prosthesis must lie beyond a certain level, because if it is too low, the two parts of the prosthesis are not bolted sufficiently; on the other side too high forces may impair the (natural) teeth where the prosthesis is attached.

2. MECHANICAL ANALYSIS OF THE SPRING

As a first approximation we calculated stresses and deformations of the spring by means of the bending theory of curved beams (see e.g. [3]). Stress concentrations arising from notches and cross section transitions were considered by a subsequent FE-analysis.

2.1 Bending Theory of Elastic Curved Beams

2.1.1 Stress and Strain

Fig. 4 shows a beam element in undeformed (left) resp. deformed state, where R and ρ denote the radii of curvature. For the sake of simplicity we assume that the curve going through the centers of gravity of the cross sections coincides with the neutral fibre. For a more general approach see [8].

Fig. 4: Beam element in undeformed and deformed state

The elastic strain is

$$\varepsilon = (\ell'-\ell)/\ell = (\rho^{-1}-R^{-1})\frac{\eta}{1+\eta\cdot R^{-1}} \qquad (1)$$

with Hooke's law we get the stress distribution

$$\sigma = E\cdot\varepsilon = E(\rho^{-1}-R^{-1})\frac{\eta}{1+\eta\cdot R^{-1}} = E(\kappa-k)\frac{\eta}{1+\eta\cdot k}\ , \qquad (2)$$

where k is the original curvature and κ is the curvature of the deformed spring (more precise: the curvature of the neutral fibre of the spring!).

2.1.2 Deformation of the spring

We wish to derive the shape of the deformed spring using "the principle of minimizing the potential enery".
With equation (2) the elastic energy density $\bar{U}$ is

$$\bar{U} = \frac{1}{2}\sigma \cdot \varepsilon = \frac{1}{2}E\varepsilon^2 = \frac{1}{2}E(\kappa-k)^2\left(\frac{\eta}{1+\eta k}\right)^2 \qquad (3)$$

and by integration over the <u>whole beam</u> the elastic energy is

$$U = \int_V \bar{U}\, dV = \frac{1}{2}E \int_0^L (\kappa-k)^2 J \ , \qquad (4)$$

where a modified moment of inertia has been introduced

$$J = \int_A \frac{\eta^2}{(1+\eta k)^2}\, dA \ , \qquad (5)$$

- A the cross section area, - L the total length of the spring. The curves of the undeformed and deformed spring are described in a cartesian coordinate system by a parametric representation $s \longmapsto (x(s),y(s))$, where s is the arc length (see fig. 5). Without loss of generality the origin can be placed in the starting point of the curve belonging to the <u>deformed</u> spring.

Fig. 5: Sketch of the undeformed and deformed spring

The curvature κ of the plain curve can be described in our special parametric representation by

$$\kappa = \langle (x,y,0)' \times (x,y,0)'' \,|\, (0,0,1) \rangle \ , \qquad (6)$$

where $(...)'$ denotes the derivative with respect to s. The angle α between x-axis and tangential vector $(x,y)'$ is given by (see fig. 6)

$$x' = \cos \circ \alpha \ , \quad y' = \sin \circ \alpha \ . \qquad (7)$$

Fig. 6: Illustration of the angle α and the tangential vector

---

Equation (6) yields $\kappa=\alpha'$. The following variational problem with constraints can be formulated

$$U = \frac{E}{2} \int_0^L (\alpha'-k)^2 J \stackrel{!}{=} \text{Min} \tag{8a}$$

with boundary conditions

$$(x,y,\alpha)(0) = (0,0,\alpha_o) \ , \quad (x,y,\alpha)(L) = (x_L,y_L,\alpha_L) \ . \tag{8b}$$

By means of the method of LANGRANGEian multipliers eq. (8a,b) is reduced to a variational problem without constraints; x(s) and y(s) in eq. (8b) can be expressed by

$$x(s) = \int_0^s \cos \circ \alpha \ , \qquad y(s) = \int_0^s \sin \circ \alpha \ . \tag{9}$$

We have to minimize

$$H(\alpha) = \int_0^L \left\{(\alpha'-k)^2 J + \lambda_1 \cos(\alpha) + \lambda_2 \sin(\alpha)\right\} \ ; \tag{10}$$

with the abbreviation

$$\hat{H}(\alpha,\alpha') = (\alpha'-k)^2 J + \lambda_1 \cos(\alpha) + \lambda_2 \sin(\alpha) \ , \tag{11}$$

our problem can be reduced to the EULER-LAGRANGE differential equation

$$\frac{\partial \hat{H}}{\partial \alpha} - \frac{d}{ds} \frac{\partial \hat{H}}{\partial \alpha'} = 0 \ . \tag{12}$$

Performing the differentiation yields

$$-\lambda_1 \sin(\alpha) + \lambda_2 \cos(\alpha) - \frac{d}{ds}\left\{2(\alpha'-k)J\right\} = 0 \ . \tag{13}$$

Rearranging equation (13) using (7) and subsequent integration leads to

$$J(\alpha'-k) = C_1 x + C_2 y + C_3 \ , \tag{14}$$

from which the system of coupled differential equations

$$\begin{aligned} \alpha' &= J^{-1}(C_1 x + C_2 y + C_3) + k \\ x' &= \cos(\alpha) \\ y' &= \sin(\alpha) \end{aligned} \tag{15}$$

follows; three additional parameters have to be determined from the boundary conditions. System (15) has to be solved numerically and yields the curve (x(s),y(s)) for the deformed spring.

2.2 Finite Element Analysis

By means of formula (2) one can derive the stress distribution within the spring and the forces which are needed to cause the "given" deflection. Nevertheless our model is a rough one; therefore, in order to get more precise information about stress concentrations, an analysis was performed with the FE-Program ADINA 5. Twodimensional solid elements were used for the modeling of the plain spring structure.

3. NEW SPRING SHAPES

By means of computer programs several spring shapes were analyzed, which unfortunately turned out to be inadequate. As mentioned earlier, the maximum loading corresponds with a deflection of 0.3 mm; this takes place when the spring is compressed completely within the chip box; the maximum stress then arising must be smaller than a critical value of the material and the spring force must be within a certain range. The calculations showed that in most of the cases one of these conditions was not satisfied, e.g. stresses $\sigma_{max} \gtrsim 1500$ N/mm^2 are not acceptable. Another problem is that manufacturing of such small parts is restricted to some special processes so that certain spring shapes can cause additional problems.
Finally, the spring shape in figure 7 turned out to be suitable. The maximum stress from the elementary bending theory was 810 N/mm^2 while the FE-Analysis yields 825 N/mm^2. The location of the maximum stress is point P_4 shown in figure 12.

The deformed and undeformed spring as calculated by the FEmethod are shown in figure 8. The elementary bending theory seems to represent a good approximation.

Fig. 7: New shape of the spring

Fig. 8: FE-analysis: deformation of the spring

---

4. MATERIAL AND MANUFACTURING PROCESS

The high stress level allows to use high strength steels only. For medical reasons this material must be stainless. Thus the spring steel X 12 CrNi 17 7 ($R_m \gtrsim 1650$ N/mm^2) or
X 5 CrNiMo 18 10 ($R_m \gtrsim 1250$ N/mm^2) can be chosen. The tensile strength R_m can be increased considerably by heat treatment. The values are valid for sheet material up to 0.25 mm [7]. Due to the small size of the spring, the choice of manufacturing processes is very restricted. Thus an etching method was chosen. The spring shape was etched out from a sheet with a thickness of 0.2 mm which is half the thickness of the final spring. Subsequently two halfs are welded together by means of a laser.

5. FRACTURE MECHANIC ASPECTS

For high strength steels the danger of brittle fracture of the structure exists. In order to exclude failure emanating from possible small cracks due to material defects or manufacturing, fracture mechanic concepts are applied. The stress intensity factor as a measure for the intensity of the singular stress field near the crack tip can be calculated from the general expression ([4])

$$K_I = \sigma\sqrt{\pi \cdot a}\; Y(a/w) \quad , \tag{16}$$

where Y is a dimensionless function taking into account the special geometry and the loading case compared to a Griffith crack in an infinite plate. w is a characteristic measure of the finite geometry and a is the crack length (see fig. 9). In the present case w is identical to the width of the beam. The function Y for bending and tension can be taken from any standard stress intensity factor handbook e.g. [5].

Fig. 9: Beam element with a crack under tensile and bending load

---

Because of the small absolute size of the spring, only small crack sizes enter into the square root expression of equation (16). Thus it turns out that the stress intensity factor K_I is much smaller than the critical value, the fracture toughness

K_{I_c}. The problem therefore represents a classical problem of stress analysis.

6. OPTIMIZATION OF THE CROSS SECTION DISTRIBUTION

Hitherto in our considerations "optimization" took place only as long as it concerns the shape of the neutral fibre, not the cross section distribution; w.r.t. this distribution an evolution strategy ([6]) has been done, described in [8]; a further "improvement" of the spring was possible.

Fig. 10: Illustration of the ranges for optimization

Fig. 11: Spring with optimized contour and FE-Mesh

Fig. 12: Comparison of the stress distribution before and after the optimization

---

7. CONCLUSIONS

A small spring which constitutes an important part of a dental attachment was investigated. The original design of this shape could not endure the high loads. After mechanical analysis and optimization a new spring shape was found. The stresses could be reduced to still a high but acceptable level for a spring steel. The spring was manufactured by means of an etching method and laser welding.
As further investigations a long duration test under practical conditions is planned in order to observe the wear and fatigue of the parts during the normal lifetime of a dental prosthesis.

8. ACKNOWLEDGEMENT

This work was supported by the Wirtschaftsministerium Rheinland-Pfalz and FR-Konstruktionselemente für Zahnprothetik GmbH & Co.

9. REFERENCES

[1] W.B. Freesmeyer, Konstruktionselemente in der zahnärztlichen Prothetik, Carl Hanser Verlag, München, Wien (1987).

[2] Deutsche Patentanmeldung "Feder eines Federriegels für eine abnehmbare ...", No. P 38 38 222.9, München (1988).

[3] H. Göldner und F. Holzweißig, Leitfaden der technischen Mechanik, 7th Edn., VEB Fachbuchverlag, Leipzig (1980).

[4] H.G. Hahn, Bruchmechanik, B.G. Teubner Verlag, Stuttgart (1976).

[5] G.C. Sih, Handbook of Stress Intensity Factors, Lehigh University Bethlehem, Pennsylvania (1973).

[6] I. Rechenberg, Evolutionsstrategie, Friedrich Frommann Verlag, Stuttgart (1973).

[7] DIN Deutsches Institut für Normung e.V., Stahl und Eisen Gütenormen Taschenbuch 4, Berlin, Köln (1975).

[8] Claus-Peter Fritzen, Peter Hackh, Pierre Hubsch, Optimization of a Spring Shape for Dental Attachments, to appear in Forensic Engineering (1990).

Figure Legend

Fig. 1: Chip-box and original spring of the FR-chip
Fig. 2: Schematic illustration of the spring position in the chip-box
Fig. 3: Application of the FR-chip in a dental prosthesis model
Fig. 4: Beam element in undeformed and deformed state
Fig. 5: Diagrammatic sketch of undeformed and deformed spring
Fig. 6: Illustration of the angle α and tangential vector
Fig. 7: New shape of the spring
Fig. 8: FE-analysis: deformation of the spring
Fig. 9: Beam element with a crack under tensile and bending load
Fig. 10: Illustration of the ranges for optimization
Fig. 11: Spring with optimized contour and FE-mesh
Fig. 12: Comparison of the stress distribution before and after optimization

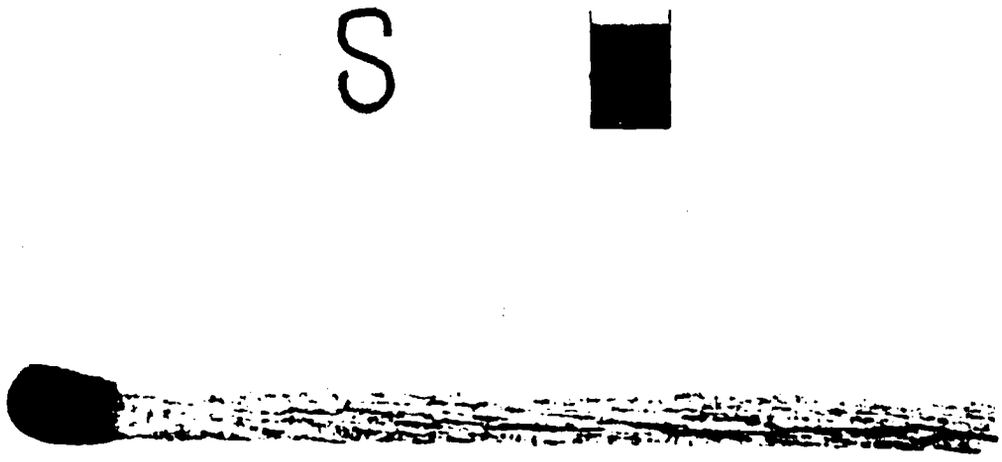

Fig. 1 : Chip -box and orignal spring of the FR-chip .

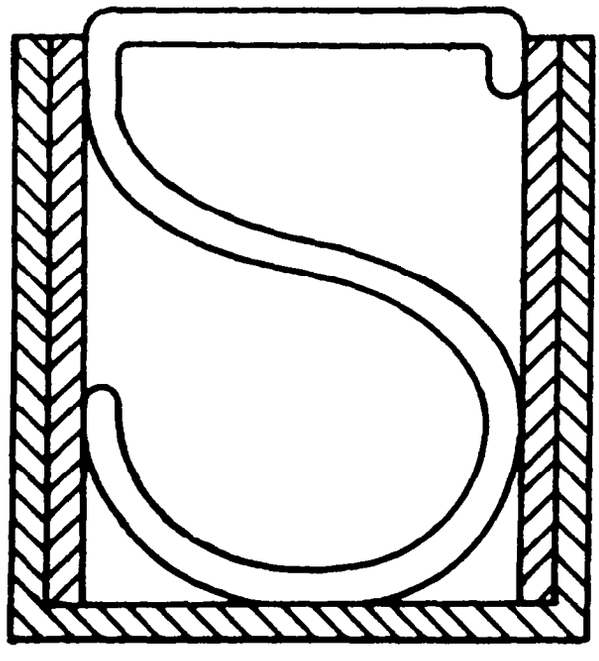

Fig. 2: Schematic illustration of the spring position in the chip-box

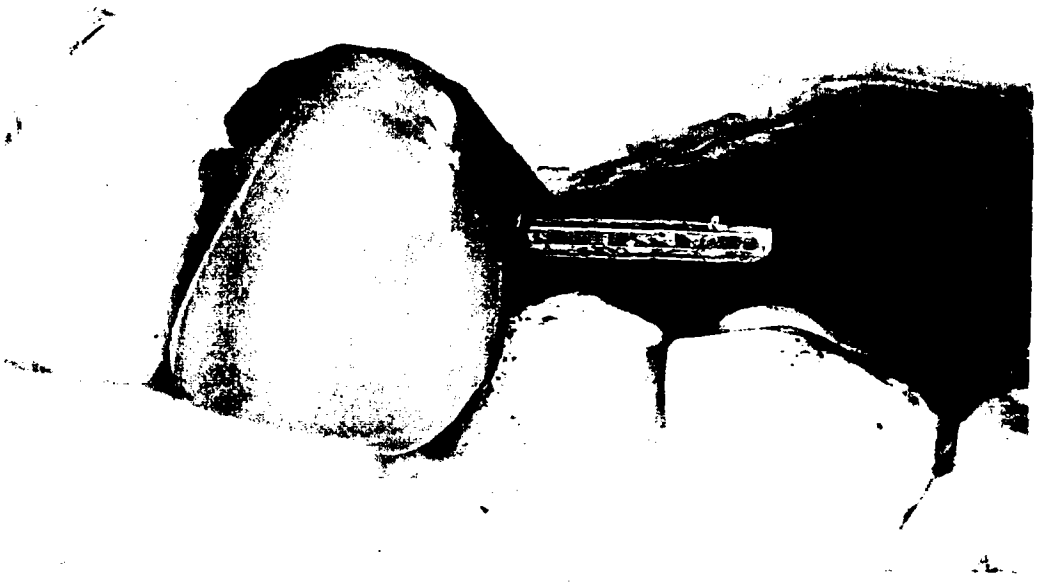

Fig. 3: Application of the FR-CHIP in a dental prosthesis model

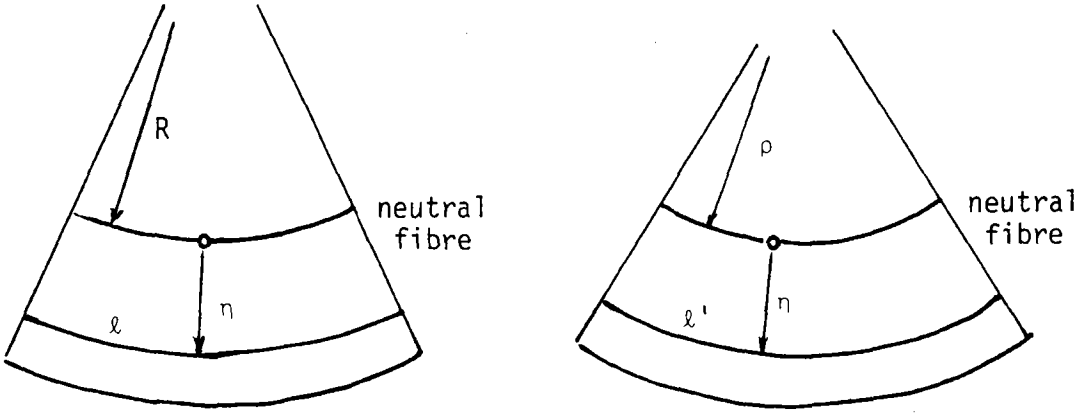

Fig. 4: Beam element in undeformed and deformed state

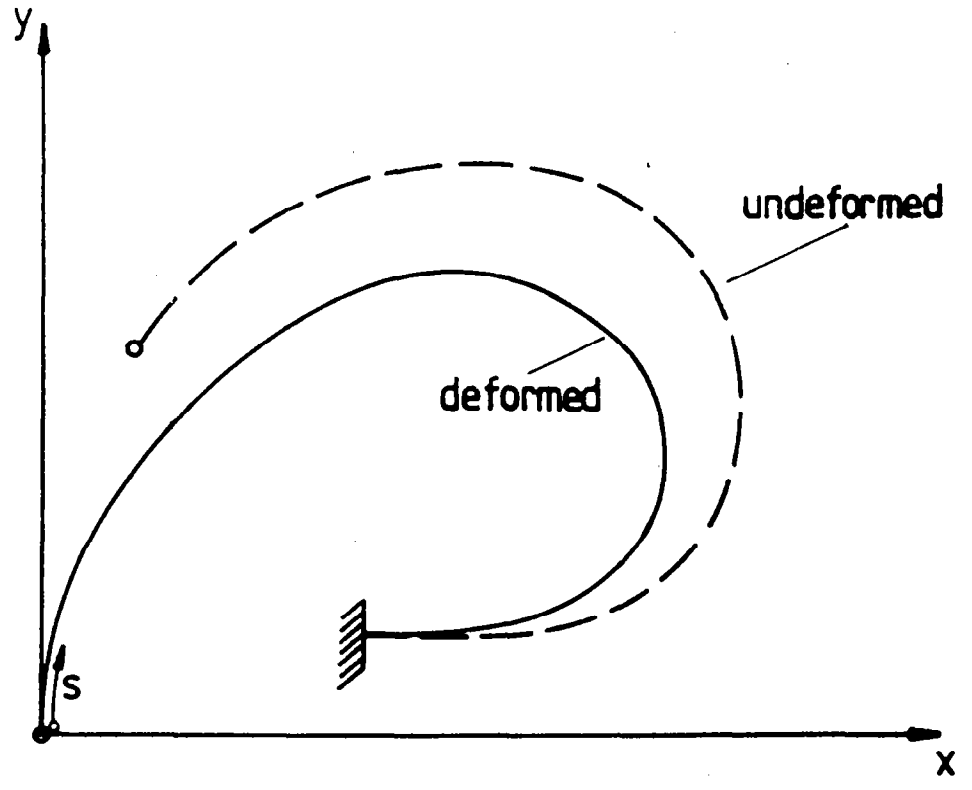

Fig. 5: Diagrammatic sketch of undeformed and deformed spring

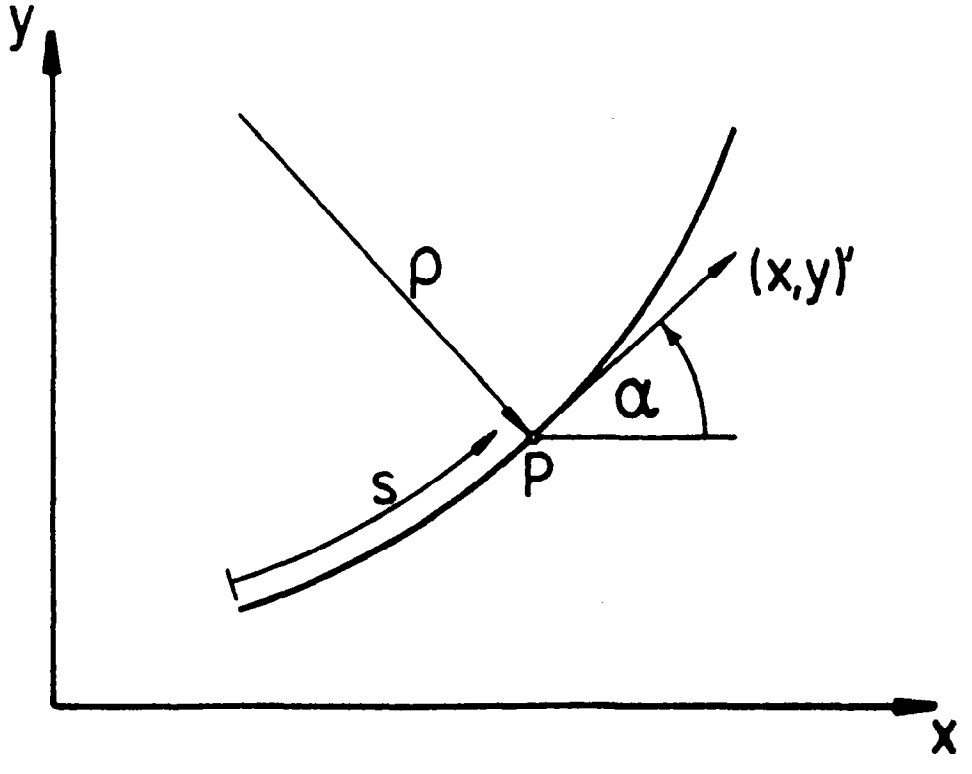

Fig. 6: Illustration of the angle α and tangential vector

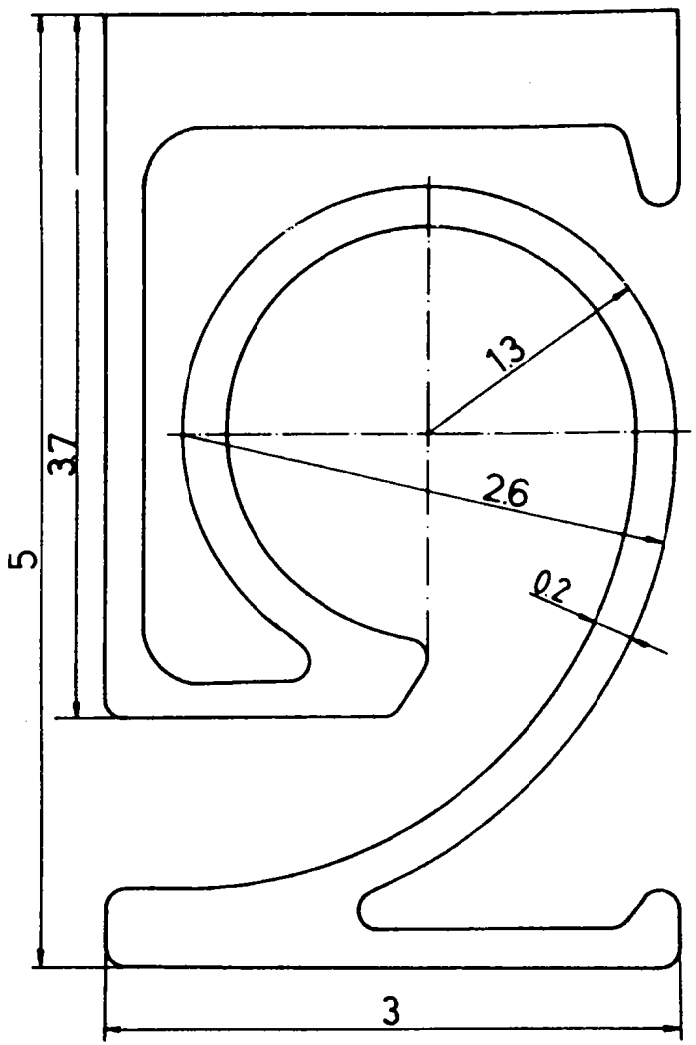

Fig. 7: New shape of the spring

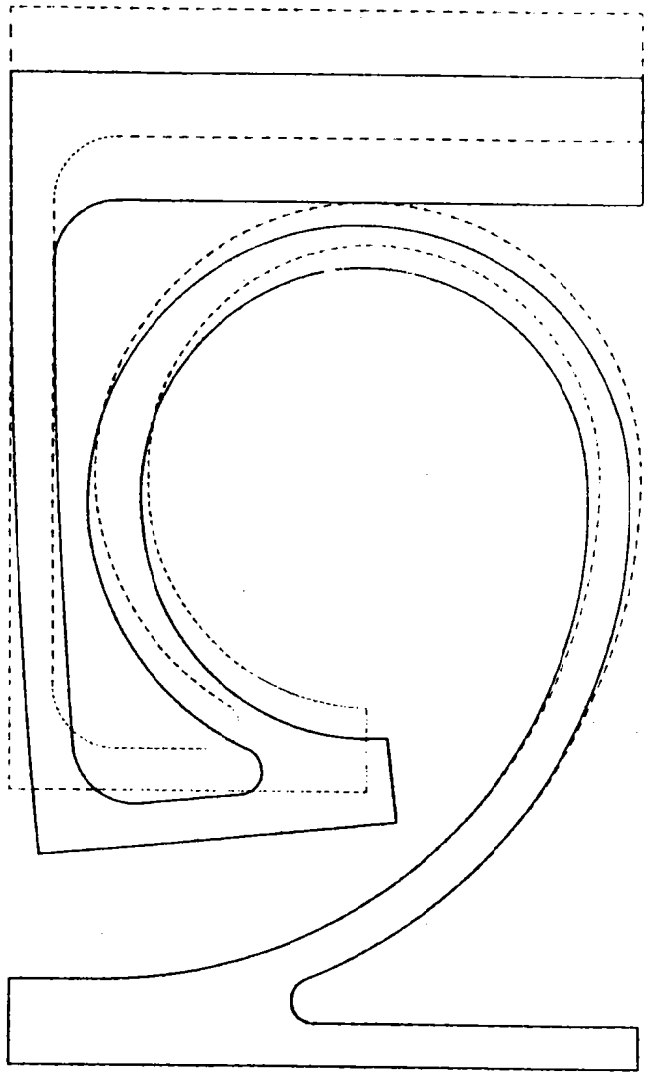

Fig. 8: FE-analysis : deformation of the spring

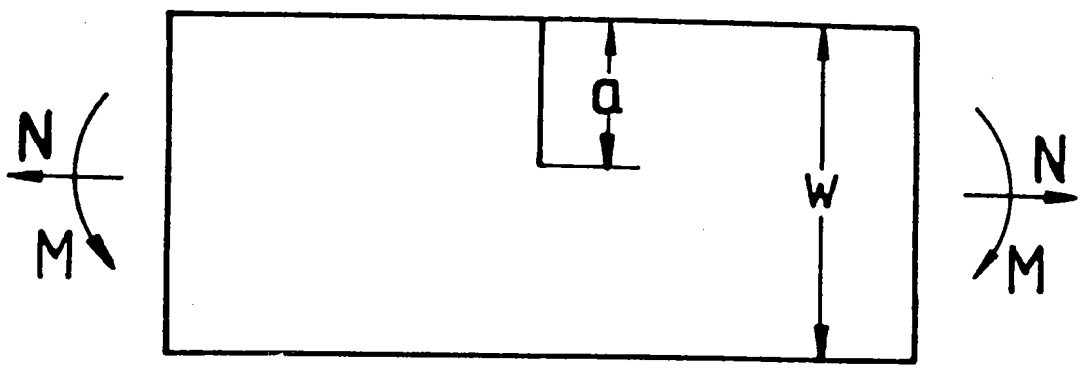

Fig. 9. Beam element with a crack under tensile and bending load

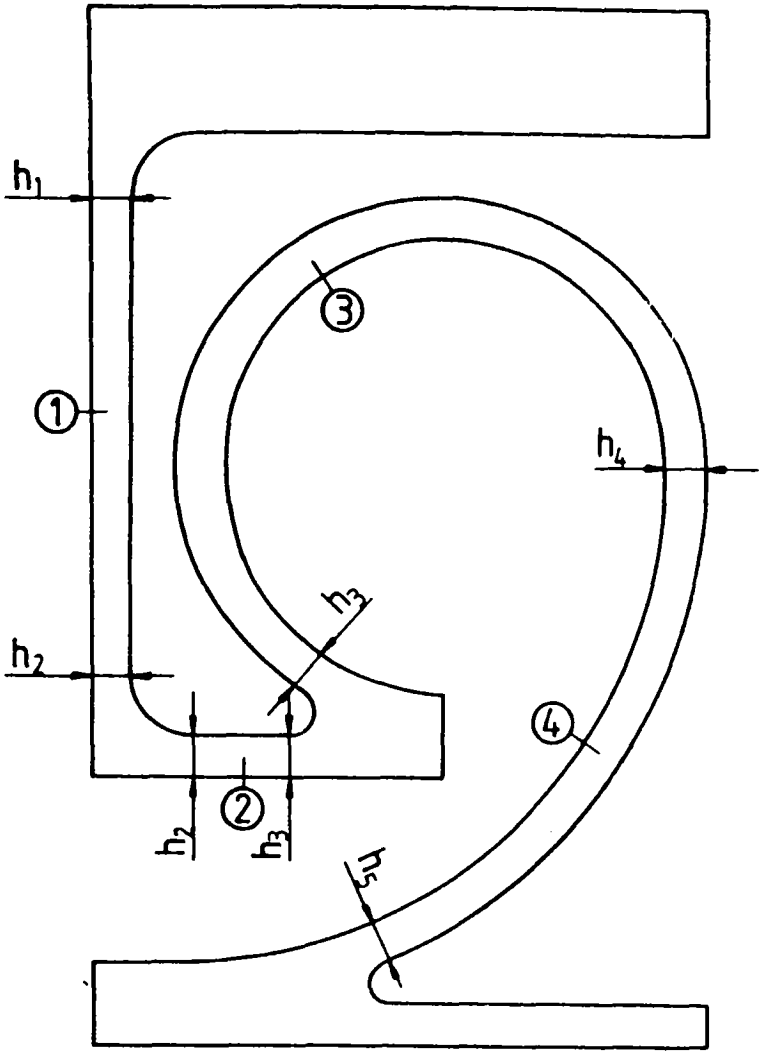

Fig. 10: Illustration of the ranges for optimization

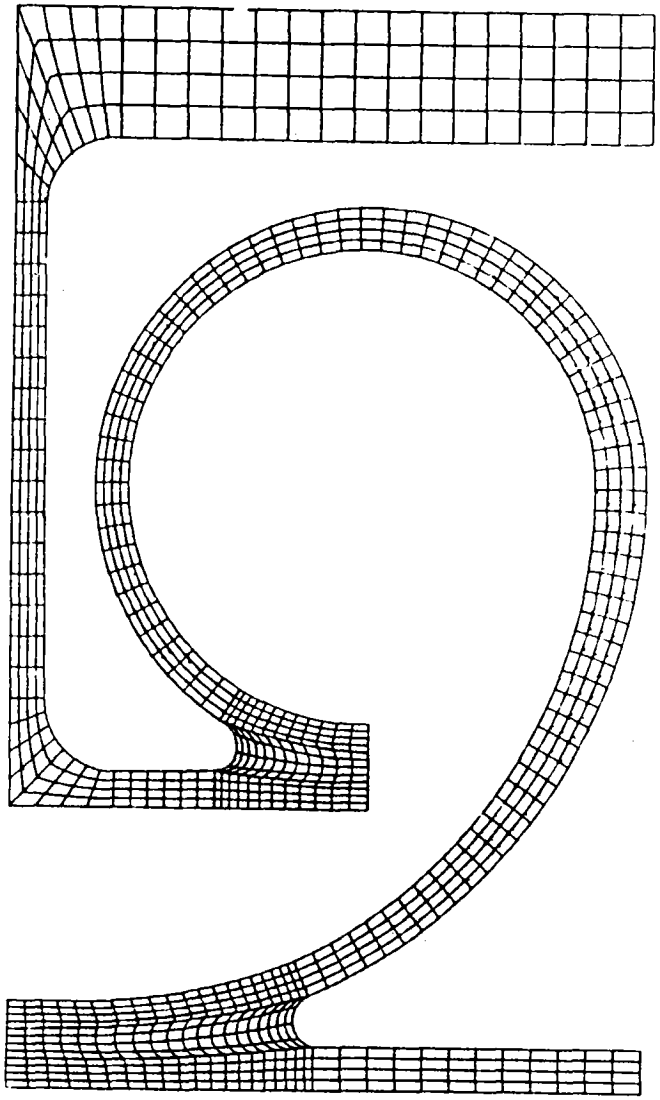

Fig. 11: Spring with optimized contour and FE-mesh

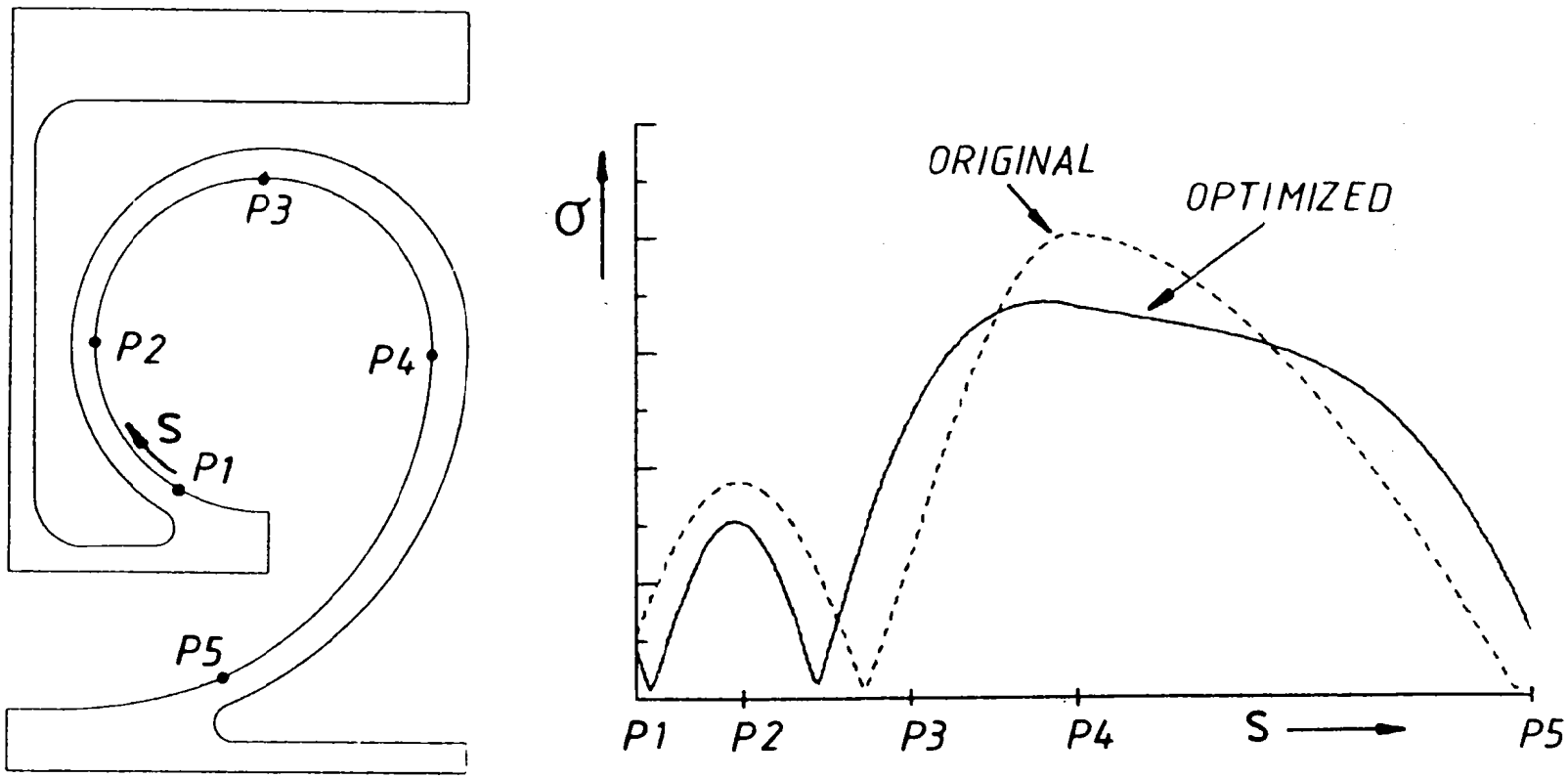

Fig. 12: Comparison of the stress distribution before and after optimization